Epigenetic silencing of Th1 type chemokines shapes tumor immunity and immunotherapy

Dongjun Peng[1], **Ilona Kryczek**[1,2], **Nisha Nagarsheth**[1,2], **Lili Zhao**[3], **Shuang Wei**[1], **Weimin Wang**[1], **Yuqing Sun**[4], **Ende Zhao**[1], **Linda Vatan**[1], **Wojciech Szeliga**[1], **Jan Kotarski**[5], **Rafał Tarkowski**[5], **Yali Dou**[4], **Kathleen Cho**[4,7], **Sharon Hensley-Alford**[8], **Adnan Munkarah**[8], **Rebecca Liu**[6,7], and **Weiping Zou**[1,2,7,9,*]

[1]Department of Surgery, University of Michigan School of Medicine, Ann Arbor, MI, USA, 48109

[2]Graduate Program in Immunology, University of Michigan, Ann Arbor, MI, USA, 48109

[3]Department of Biostatistics, University of Michigan School of Medicine, Ann Arbor, MI, USA, 48109

[4]Department of Pathology, University of Michigan School of Medicine, Ann Arbor, MI, USA, 48109

[5]The First Department of Gynecologic Oncology and Gynecology, Medical University in Lublin, Poland, 20-081

[6]Department of Obstetrics and Gynecology, University of Michigan School of Medicine, Ann Arbor, MI, USA, 48109

[7]The University of Michigan Comprehensive Cancer Center, University of Michigan, Ann Arbor, MI, USA, 48109

[8]Department of Women's Health Services, Henry Ford Health System, Detroit, MI, USA, 48202

[9]Graduate Program in Tumor Biology, University of Michigan, Ann Arbor, MI, USA, 48109

Summary

Epigenetic silencing including histone modifications and DNA methylation is an important tumorigenic mechanism[1] However, its role in cancer immunopathology and immunotherapy is poorly understood. Using ovarian cancers as our model, we found that enhancer of zeste homolog 2 (EZH2)-mediated histone H3 lysine 27 trimethylation (H3K27me3) and DNA methyltransferase (DNMT) 1-mediated DNA methylation repress the tumor production of Th1-type chemokines CXCL9 and CXCL10, and subsequently determine effector T cell trafficking to the tumor microenvironment. Treatment with epigenetic modulators removes the repression and increases effector T cell tumor infiltration, slows down tumor progression, and improves therapeutic efficacy

---

of PD-L1 (B7-H1) checkpoint blockade[2–4] and adoptive T cell transfusion[5] in tumor bearing mice. Moreover, tumor EZH2 and DNMT1 are negatively associated with tumor infiltrating CD8^{+} T cells and patient outcome. Thus, epigenetic silencing of Th1-type chemokine is a novel tumor immune evasion mechanism. Selective epigenetic reprogramming alters T cell landscape[6] in cancer and may enhance clinical efficacy of cancer therapy.

Keywords

Chemokine; CXCL9; CXCL10; trafficking; EZH2; DNMT; histone modification; DNA methylation; epigenetics; chemotherapy; T cell therapy; PD-1; PD-L1; B7-H1; checkpoint; cancer

Cancer immunotherapy has demonstrated therapeutic responses [4,5,7,8]. Yet, the objective responses have been manifested in a fraction of patients. We hypothesized that immune protective signature genes might be epigenetically silenced in cancer and in turn affect cancer progression and clinical responses to immunotherapy. Cancer epigenetic silencing often includes EZH2-mediated histone modifications and DNMT mediated-DNA methylation. DZNep [9] is an inhibitor of all SAM dependent enzymes including EZH2 and EPZ6438 [10] may specifically inhibit EZH2. 5-aza-2′deoxycytidine (5-AZA dC) is a DNMT inhibitor. Hence, we used these agents to reprogram epigenetic pathways and to test our hypothesis.

In the first setting, we established ID8 ovarian cancer in C57/BL6 mice and treated them with low doses of DZNep and EPZ6438, 5-AZA dC and their combination. Treatment with single agent had minimal effects on tumor volume, whereas the combinatorial treatment caused tumor reduction, increased tumor infiltrating T cells and Th1-type chemokine expression (Extended Data Fig. 1a–e). We observed similar tumor volume (Extended Data Fig. 1f) in ID8 bearing, female NOD-scid IL2Rγnull (NSG) mice [11], that received identical treatment. Thus, epigenetic reprograming elicits potent tumor immunity and blocks cancer progression.

We have demonstrated the relevance of the inhibitory B7-H1 (PD-L1) signaling blockade in human cancer [2,3]. In the second setting, we tested the role of DZNep and 5-AZA dC in anti-tumor immunity elicited by PD-L1 blockade. We observed reduced tumor volume in mice treated with anti-PD-L1 or DZNep plus 5-AZA dC. The combination reduced tumor volume, increased tumor infiltrating CD8^{+} T cells and Th1-type chemokine expression (Extended Data Fig. 1g–i). Thus, changes in epigenetic program can augment therapeutic efficacy of PD-L1 blockade therapy.

In the third setting, we examined the effects of these two epigenetic modulators on adoptive T cell therapy in our NSG model. We established human ovarian cancer in NSG mice and generated tumor associated antigen (TAA)-specific CD8^{+} T cells [12–14]. Then, the NSG mice were treated with DZNep and 5-AZA dC, and/or TAA-specific CD8^{+} T cells. In the absence of TAA-specific T cells, treatment with DZNep and 5-AZA dC had minimal effects on tumor progression. TAA-specific CD8^{+} T cells reduced tumor volume (Extended Data Fig. 1j). Consequently, treatment with DZNep and 5-AZA dC improved the therapeutic efficacy of T cell therapy, and elevated Th1-type chemokine expression, and tumor effector T cells

(Extended Data Fig. 1j–l). GSK126 is a selective inhibitor of EZH2 methyltransferase activity [15]. We use GSK126 in the human T cell therapy setting. Treatment with low doses of GSK126 and/or 5-AZA dC had no effect on tumor growth in the absence of T cell transfusion (Extended Data Fig. 1m). Treatment with GSK126 and 5-AZA dC synergistically improved the therapeutic efficacy of T cell therapy (Fig. 1a, Extended Data Fig. 1m), increased tumor CXCL9 and CXCL10 expression (Fig. 1b, c), and CD8$^+$ T cell infiltration (Fig. 1d, e, Extended Data Fig. 1n), and had minimal effects on TNFα and IFNγ expression (Extended Data Fig. 1o–q). Administration of anti-human CXCR3 abrogated the role of GSK126 and 5-AZA dC treatment in tumor progression (Fig. 1a), and blocked T cell tumor trafficking (Fig. 1d, e), and had no effect on T cell apoptosis (Extended Data Fig. 1r, s). CXCR3$^+$CD8$^+$ T cells were in spleen (Extended Data Fig. 1t) and blood (Fig. 1e) with or without anti-CXCR3 treatment. To determine the major source of Th-1 type chemokine, we isolated human tumor and immune cells from tumor tissues in the NSG mice (Fig. 1a–e). We found that administration of GSK126 and 5-AZA dC increased tumor CXCL10 expression with or without T cell transfusion (Fig. 1f). Regardless of the treatment, the levels of CXCL10 expression were higher in tumor than immune cells (Fig. 1f). We extended our studies to tumor and immune cells from ovarian cancer patients. Although EZH2 may regulates naïve CD4$^+$ T cell IFNγ expression [16], GSK126 and 5-AZA dC treatment increased CXCL10 production by tumor, not by T cells (Fig. 1g), and tumor cells produced higher levels of CXCL10 than immune cells (Fig. 1g). Thus, epigenetic reprograming may predominantly target tumor Th1-type chemokine expression.

Next, we investigated how epigenetic modulators regulate tumor Th1-type chemokine expression. We initially examined the effect of DZNep on Th1-type chemokine expression in primary human ovarian cancer cells in response to IFNγ treatment. DZNep promoted CXCL9 and CXCL10 mRNA and protein expression (Extended Data Fig. 2a–c), and had no effect on IFNγ receptor (IFNGR2) (Extended Data Fig. 2d). We tested two inhibitors of histone H3 lysine 9 methyltransferase G9a, BIX01294 and UNC0638. The inhibition of G9a had no effects on the Th1-type chemokine expressions (Extended Data Fig. 2e). Thus, methylation of H3K27 may mediate Th1-type chemokine repression in cancer.

EZH2 is the catalytic subunit of the H3K27 methyltransferase complex [9,17]. DZNep treatment caused the reduction of EZH2 protein and H3K27 trimethylation (H3K27me3) in primary ovarian cancer cells (Extended Data Fig. 2f). Similarly, EPZ6438 reduced H3K27me3 expression and increased CXCL9 expression in mouse ID8 cells (Extended Data Fig. 2g, h). We genetically knocked down human EZH2 expression with lentivirus-based short hairpin RNA for EZH2 (shEZH2). shEZH2 reduced the expression of EZH2 and H3K27me3 (Extended Data Fig. 2i), and resulted in elevated Th1-type chemokine mRNA and protein expression (Fig. 2a, b), and no change in IFNGR2 and HLA-B (Extended Data Fig. 2j, k). Thus, EZH2 and its histone methyltransferase activity mediate Th1-type chemokine repression in primary ovarian cancer cells.

We tested whether EZH2 mediated Th1-type chemokine repression depends on H3K27me3 changes at the promoter level. Chromatin immunoprecipitation (ChIP) assay revealed that IFNγ treatment reduced H3K27me3 levels on the promoters of CXCL9 and CXCL10 (Extended Data Fig. 2l, m). DZNep (Extended Data Fig. 2l, m) and shEZH2 (Fig. 2c) largely

removed H3K27me3 occupancy on the promoters of CXCL9 and CXCL10, and subsequently increased IFNγ-induced chemokine gene expressions (Fig. 2a, b). As a positive control, shEZH2 reduced H3K27me3 occupancy on the promoter of HOXB1 gene (Extended Data Fig. 2n)[18]. Thus, H3K27me3 removal results in the abrogation of the Th1-type chemokine gene silencing in primary ovarian cancer.

GSK126 is a selective inhibitor of EZH2 methyltransferase activity [15]. GSK126 treatment abolished the global level of H3K27me3 without inhibiting EZH2 (Extended Data Fig. 3a, b), IFNGR2 expression and cell survival (Extended Data Fig. 3c, d). GSK126 treatment led to higher levels of IFNγ-induced Th1-type chemokine expression in two primary and three established ovarian cancer cell lines (Fig. 2d, Extended Data Fig. 3e–h). JmjC-domain-containing protein, JMJD3 is an H3K27 specific demethylase [18]. Ectopic expression of JMJD3 reduced H3K27me3 (Extended Data Fig. 3i), and increased Th1-type chemokine expression (Fig. 2e, Extended Data Fig. 3j), and had no effect on HLA-B and IFNGR expression (Extended Data Fig. 3k, l). JMJD3 deficiency introduced by a shJMJD3 inhibited CXCL10 (Fig. 2f), but not IFNGR expression (Extended Data Fig. 3m).

GSK-J4, a catalytic site inhibitor, may target H3K27-specific JmjC demethylase subfamily [19]. GSK-J4 treatment increased H3K27me3 (Extended Data Fig. 3n) and reduced CXCL9 and CXCL10 expression (Fig. 2g), had no effects on H3K4me1, H3K4me2 and H3K4me3 and IFNGR expression (Extended Data Fig. 3n, o).

To define the gene profile altered by EZH2 and H3K27me3 in response to IFNγ, we performed several microarrays in primary ovarian cancer cells transfected with shEZH2, control, or treated with GSK126 and medium. We found that 155 and 124 genes were altered by shEZH2 and GSK126 treatment, respectively, and 20 genes were increased or decreased by both shEZH2 and GSK126 treatment. CXCL9 and CXCL10 were at the top 1 and 3 positions among the increased genes in the arrays (Fig. 2h). Altogether, the data indicate that H3K27me3 specific methyltransferase and demethylase preferentially and predominantly regulate Th1-type chemokine repression in primary ovarian cancer cells.

DNA methylation regulates gene expression through DNA methyltransferases (DNMTs). We treated two primary and one established ovarian cancer cell line with 5-AZA dC. 5-AZA dC treatment increased CXCL9 and CXCL10 mRNA and protein expression (Fig. 3a–c, Extended Data Fig. 4a–d). IRF1 and IFNGR were not affected by 5-AZA dC treatment (Extended Data Fig. 4e, f). Specific knockdown of DNMT1 (Extended Data Fig. 4g) increased CXCL9 and CXCL10 mRNA and protein (Fig. 3d–f), but had no effects on IFNGR2 (Extended Data Fig. 4h). To demonstrate DNA methylation status in the CXCL10 locus, we carried out bisulfite genomic sequencing on the CXCL10 gene locus and analyzed the methylation at the CXCL10 gene loci containing STAT1 binding site (Fig. 3g, Extended Data 4i). The genomic location of bisulfite sequencing was at 5′ upstream of the CXCL10 gene promoter (−5 kb to −4.7 kb). 5-AZA dC treatment reduced DNA methylation of the CXCL10 gene locus (Fig. 3g). Thus, DNA methylation regulates Th1-type chemokine expression.

We examined the relationship between EZH2/H3K27me3 and DNA methylation in the regulation of chemokine expression. We treated primary ovarian cancer cells with 5-AZA dC or GSK126, and found that 5-AZA dC reduced DNMT1 expression but had no effects on H3K27me3 and H3K9me2, whereas GSK126 reduced H3K27me3 expression but had no effects on DNMT1 expression (Fig. 4a). Thus, DNA methylation and EZH2/H3K27me3 histone modification may not reciprocally regulate at the protein levels in primary ovarian cancer. We explored whether EZH2/H3K27me3 and DNA methylation could independently mediate the Th1-type chemokine repression. We examined the effects of 5-AZA dC on shEZH2 cells, and observed that 5-AZA dC enhanced CXCL10 expression (Fig. 4b). Similarly, GSK126 increased CXCL10 expression in shDNMT1 cells (Fig. 4c). Primary ovarian cancer cells released higher levels of CXCL10 in the combinatorial treatment of DZNep and 5-AZA dC compared to either treatment alone (Fig. 4d). The data suggest that H3K27me3 and DNA methylation can independently repress tumor Th1-type chemokine expression.

We studied the interaction between EZH2 and DNMT1 in the ovarian cancer microenvironment and its clinical relevance (Extended Data Table 1). We quantified the nuclear levels of EZH2 and DNMT1 (Extended Data Fig. 5a, b) via immunohistochemistry in human ovarian cancer tissues by the H-score method[11] and analyzed their impact on patient survival (Extended Data Table 1). Based on the median values of EZH2 and DNMT1 intensity, we divided patients into "low" and "high" groups. Overall survival (OS) and disease free-interval (DFI) (Extended Data Table 1) were shorter in patients with high levels of EZH2 (Fig. 4e, Extended Data Fig. 5c) and DNMT1 (Fig. 4f, Extended Data Fig. 5d) compared to patients with low levels of these marks. After adjusting for the prognostic clinical factors, OS and DFI remained shorter in patients with high EZH2 and DNMT1 expression (Extended Data Table 2). Tumor EZH2 and DNMT1 were positive predictors of death hazard in univariate (Extended Data Table 1) and multivariate analyses (Extended Data Table 2). The reduced OS and DFI were more pronounced in the combination of high levels of EZH2 and DNMT1 than EZH2 or DNMT1 alone (Extended Data Table 3).

To estimate the performance of EZH2 and DNMT1 on predicting survival, we used the time-dependent receiver operating characteristic (ROC) curve analysis[20]. The area under the ROC curve (AUC) is calculated to evaluate the predictive accuracy of each marker for estimating survival. The analysis revealed similar AUCs for EZH2 and DNMT1 in predicting OS and DFI (Fig. 4g, Extended Data Fig. 5e and Table 4). The expression of EZH2 and DNMT1 may be equally important in ovarian cancer pathology. Next, we evaluated significance of the two parameters for ovarian cancer survival. Given the negative and independent impact of EZH2 and DNMT1, we reasoned that both parameters are more efficient at predicting survival than individually. Indeed, EZH2^{high}DNMT1^{high} patients experienced a shorter OS and DFI (Extended Data Table 3) than EZH2^{low}DNMT1^{low} patients in univariate and multivariate analysis (Fig. 4h). Patients with mixed patterns had similar and moderate survival (Fig 4h, Extended Data Fig. 5f). Thus, the combination of EZH2 and DNMT1 allows for improved prognostic stratification of ovarian cancer survival as compared to EZH2 or DNMT1 alone. Next, we quantified intratumoral CD8$^+$ T cells by immunohistochemistry (Extended Data Fig. 5g), and found that there was a correlation between tumor CD8$^+$ T cell content and survival (Extended Data Table 1, 2). We divided the

patients into two groups based on the median values of CD8^{+} T cell number. Patients with the higher CD8^{+} T cells experienced longer OS and DFI compared to those with fewer CD8^{+} T cell group [21,22] (Fig. 4i, Extended Data Fig. 5h). ROC curve analysis revealed similar power of CD8^{+} T cells in predicting OS (Fig. 4g) and DFI (Extended Data Fig. 5e).

Finally, we observed that the levels of EZH2 (Fig. 4j) and DNMT1 (Fig. 4k) were inversely associated with CD8^{+} T cells, respectively. The accumulating levels of EZH2 and DNMT1 negatively correlated with intratumoral CD8^{+} T cells (Fig. 4l). Altogether, the results suggest that tumors co-opt certain epigenetic pathway, silence Th1-type chemokine expression and repress T cell tumor homing, which functions as a novel immune evasion mechanism.

To maintain cellular identity, through epigenetic mechanisms, key stemness genes may be repressed in somatic cells, and key effector genes may be silenced in stem cells[23,24]. Tumor cells may gain stem cell properties[11]. This may explain why Th1-type chemokines, as effector genes, are repressed in cancer. Epigenetic silencing is an intrinsic tumorigenic mechanism[1]. We propose a unifying model of cancer in which epigenetic dysregulation plays biological and immunological dual roles in supporting tumor progression. Cancer immunotherapies[4,5,7,8,25] and classic therapies[26–28] rely on efficient T cell tumor trafficking, and may induce or/and expand mutated TAA-specific T cells[29,30]. Applicably, our work suggests that epigenetic reprograming may condition tumor from poor T cell infiltration to rich T cell infiltration[6], and ultimately potentiate cancer therapy (Extended Data Fig. 5i).

Methods

Ovarian cancer patients, cancer tissue samples and primary ovarian cancer cells

Patients diagnosed with high grade serous ovarian carcinomas were recruited for this study. Human subject use in this study was approved by the local Institutional Review Boards and the informed consents were obtained from the patients. We collected 186 formalin-fixed, paraffin-embedded ovarian tumor tissue blocks (Extended Data Table 1) and 20 fresh ovarian cancer tissues for this study as described previously[2,12,31]. After pathological review, a tissue microarray (TMA)[11,32] was constructed from the most representative area of paraffin-embedded ovarian tumor tissue. For each tumor, a minimum of two representative tumor areas were selected from a hematoxylin- and eosin-stained section of a donor block. Core cylinders (1 mm) were punched from each of these areas and deposited into a recipient paraffin block. Consecutive 6 μm-thick TMA sections were cut and placed on charged Poly-L-Lysine-coated slides for immunohistochemistry analyses. Further information regarding the TMA is described in the supplementary experimental procedures. Epithelial cell adhesion molecule expressing (EpCAM^{+}) primary tumor cells, CD14^{+}CD45^{+} macrophages, CD3^{+}CD45^{+} T cells, and CD45^{+} immune cells were isolated and sorted from fresh ovarian cancer tissues for functional studies. Primary human ovarian cancer cell lines (OC8 and OC17) were generated from fresh ovarian cancer tissues and/or ascites fluid in our laboratory as previously described[11,13,33]. Three commercialized ovarian cancer cell lines A2780, CAOV3 and ES-2 were included in the study. The cell lines were routinely tested for mycoplasma contamination. All the commercialized cell lines were authenticated by the

supplier and used within 10 passages. Primary ovarian cancer cells were authenticated in the laboratory.

Plasmids, shRNA and antibodies

pCMV-HA-JMJD3 plasmid was obtained from Addgene (#24167). Lentiviral shRNAs (Extended Data Table 5) were provided by the Vector Core at the University of Michigan or kindly provided by Dr. Arul Chinnaiyan (University of Michigan). Antibodies including monoclonal anti-EZH2 (1:2000, BD Biosciences, 612667), anti-H3K27me3 (1:1000, Millipore, 07-449), H3K9me2 (1:2000, ab1220, Abcam), H3K9me3 (1:500, ab8898, Abcam), H3K4me1 (ab8895, Abcam), H3K4me2 (ab194678, Abcam), H3K4me3 (ab1012, Abcam), anti-Histone H3 (1:2000, Cell Signaling, 9715), anti-HA (1:200, Santa Cruz Biotechnology, sc-805), anti-DNMT1 (1:250, Abcam, ab13537) were used for Western blotting. Anti-human CXCR3 (1C6) blocking antibody was prepared from mouse hybridoma (ATCC, #HB-12330) by Hybridoma Core at the University of Michigan.

Quantitative Real-Time RT-PCR and Microarray

RNA exacted with Trizol (Invitrogen) was used for cDNA synthesis with high capacity cDNA reverse transcript kit (Applied Biosystems, 4374966). Real-time RT-PCR was performed on the Eppendorf Realplex Real-Time PCR system or StepOne Plus Real-Time PCR system (Life Technologies). The mRNA was quantified and normalized to the amount of GAPDH. The specific primers used for Real-Time PCR are listed in the Extended Data Table 5.

Gene expression microarray was carried out at the University of Michigan Microarray Core Facility using Affymetrix Human Gene ST 2.1 Chip according to the standard protocol. Data was analyzed by the University of Michigan Bioinformatics Core Facility. Two biological replicates of each sample were prepared independently from primary human ovarian cancer cells for gene expression profiling. Genes with >1.5 fold changes were selected for further analysis.

Chromatin immunoprecipitation (ChIP)

ChIP assay was described previously [11,32]. Sonication was performed with the Misonix 4000 water bath sonication unit at 15% amplitude for 10 minutes. ChIP-enriched chromatin was analyzed by Real-Time PCR with SYBR Green Master Mix, and normalized to the input. The ChIP primers were listed in the Extended Data Table 5.

Immunofluorescence staining (IF) and Immunohistochemistry staining (IHC)

Mouse tumor xenografts were harvested and either fixed in 10% buffered formalin and embedded in paraffin for immunohistochemistry assay, or immediately frozen and embedded in OCT compound embedding medium for immunofluorescence staining. The immunofluorescence staining was performed with the monoclonal anti-CD8 (HIT8a, #550372, BD Biosciences). Alexa Fluor 488 or Alexa Fluor 563 conjugated anti-mouse secondary antibodies (Life Technologies) were used. Staining with isotype antibody was used as negative control. T cells were counted manually at 10 ~ 20 high-power fields under Fluorescence Microscope (Leica). Immunohistochemical staining on human TMA slides or

frozen ovarian cancer tissue sections was performed on a DAKO Autostainer (DAKO) using DAKO LSAB+ and diaminobenzadine (DAB) as the chromogen. Serial sections of de-paraffinized TMA sections were labeled with rabbit anti-human EZH2 antibody (Clone ZMD.309, 18-7395, 1:200, Life Technologies), rabbit anti-DNMT1 (Clone H-300, sc-20701, 1:50, Santa Cruz Biotechnology), and mouse anti-human CD8 antibody (DAKO, M7103). Cores from several normal organ tissues were used as tissue controls on each slide.

The cores were quantified and analyzed for the expression of EZH2 and DNMT1 with an Aperio imaging system (Genetix) and for the numbers of intratumoral CD8+ T cells in 0.1 mm^2 tumor. The specimens were digitalized with an automated platform (Aperio Technologies) and ScanScope XT and Spectrum Plus using TMA software version 9.1 scanning system. Cores were scored in high resolution of 40X. Tissue sections were scored manually on a computer screen, and a mean score for duplicate cores from each individual was calculated. Any discrepancies were resolved by subsequent consultation with diagnostic pathologists. Epigenetic marks, EZH2 and DNMT1 were localized in the nuclei, and were scored using the H-score method [11,32]. The tissues were divided into high and low epigenetic mark expression based on the median value of the expression level per core. The H-score is a method of assessing the extent of nuclear immunoreactivity. The H score takes into account the percentage of positive cells (0–100%) in each intensity category (0–3+) and computes a final score, on a continuous scale between 0 and 300. The score is obtained by the formula: 3 x percentage of strongly staining nuclei + 2 x percentage of moderately staining nuclei + percentage of weakly staining nuclei, giving a range of 0 to 300 [11]. Staining with isotype antibody was used as negative control.

In vivo tumor progression and immunotherapy models

ID8 mouse ovarian cancer cells were described originally [34]. ID8 cells (5 x 10^5) were injected into peritoneal cavity of NSG mice or C57BL/6 mice (6–8 weeks old, Jackson Lab) [11,32]. Tumor progression was monitored 2 ~ 3 times per week by Xenogen IVIS® Spectrum in vivo Bioluminescence imaging system (PerkinElmer). Tumor volume was calculated based on the total flux (photons per second). Tumor-bearing mice were treated (i. p) with 5 mg/kg DZNep (SML0305, Sigma), 50 mg/kg EPZ6438 (E-7438, Active Biochem), 0.2 mg/kg 5-AZA dC (A3656, Sigma), or 10 mg/kg anti-PD-L1 (B7-H1, clone 10F.9G2, BE0101, Bio X Cell) three times per week for two weeks. In some cases, tumor was dissected for the analysis of chemokine production or T cells infiltration as indicated.

In adoptive T cell therapeutic model, human TAA-specific CD8+ T cells were generated in vitro and primary human ovarian cancer cells were inoculated subcutaneously into the flanks of NSG mice [11,32]. TAA-specific CD8+ T cells (7 X 10^6) were intravenously transfused into tumor-bearing mice. DZNep (5 mg/kg), GSK126 (30 mg/kg), and 5-AZA dC (0.2 mg/kg) treatments were started before T cell transfusion by intraperitoneal administration 3 times per week. In some cases, mice received CD8+ T cells which were preincubated with anti-CXCR3 for 1 hour before in vivo transfusion, followed by intraperitoneal administration of 500 µg anti-CXCR3 for 3 times per week. Tumor growth was monitored and recorded. Tumor cells and tumor infiltrating immune cells were isolated and studied by FACS, real-

time PCR and/or immunohistochemistry. All animal protocols were approved by the University of Michigan Committee on Use and Care of Animals (UCUCA).

Statistical analysis

Wilcoxon rank-sum tests were used to compare two independent groups, and for paired groups, Wilcoxon signed rank tests were used for the comparison. Correlation coefficients (Spearman correlation, denoted by r, for ordinal data and Pearson correlation, denoted by r, for continuous data), together with a P-value (null hypothesis is that r is in fact zero), were computed to measure the degree of association between biomarkers. Log-rank test was used to compare time to tumor initiation between two groups. Overall patient survival was defined as the time from date of diagnosis and to disease related death. Survival functions were estimated by Kaplan-Meier methods.

Cox's proportional hazards regression was performed to model survival as a function of EZH2, DNMT1 and CD8$^+$ T cells. The data were analyzed as continuous or categorized values and classified as low and high based on the median values, or the combination of EZH2 and DNMT1 (classified as EZH2^{high}DNMT1^{high} and EZH2^{low}DNMT1^{low}), after adjusting for age and stage. We assessed the adequacy of the Cox regression model. Graphical and numerical methods were described [35]. We used ROC analysis [20] to evaluate the predictive accuracy of the levels of EZH2 and DNMT1, and CD8$^+$ T cells for 60 month survivals. All analyses were done using SAS 9.3 software. P < 0.05 considered as significant. No statistical methods were used to predetermine sample size. Sample size was determined on the basis of animal experimental trials and in consideration of previous publications on similar experiments to allow for confident statistical analyses. The experiments were not randomized. The investigators were not blinded to allocation during experiments and outcome assessment unless state differently.

Extended Data
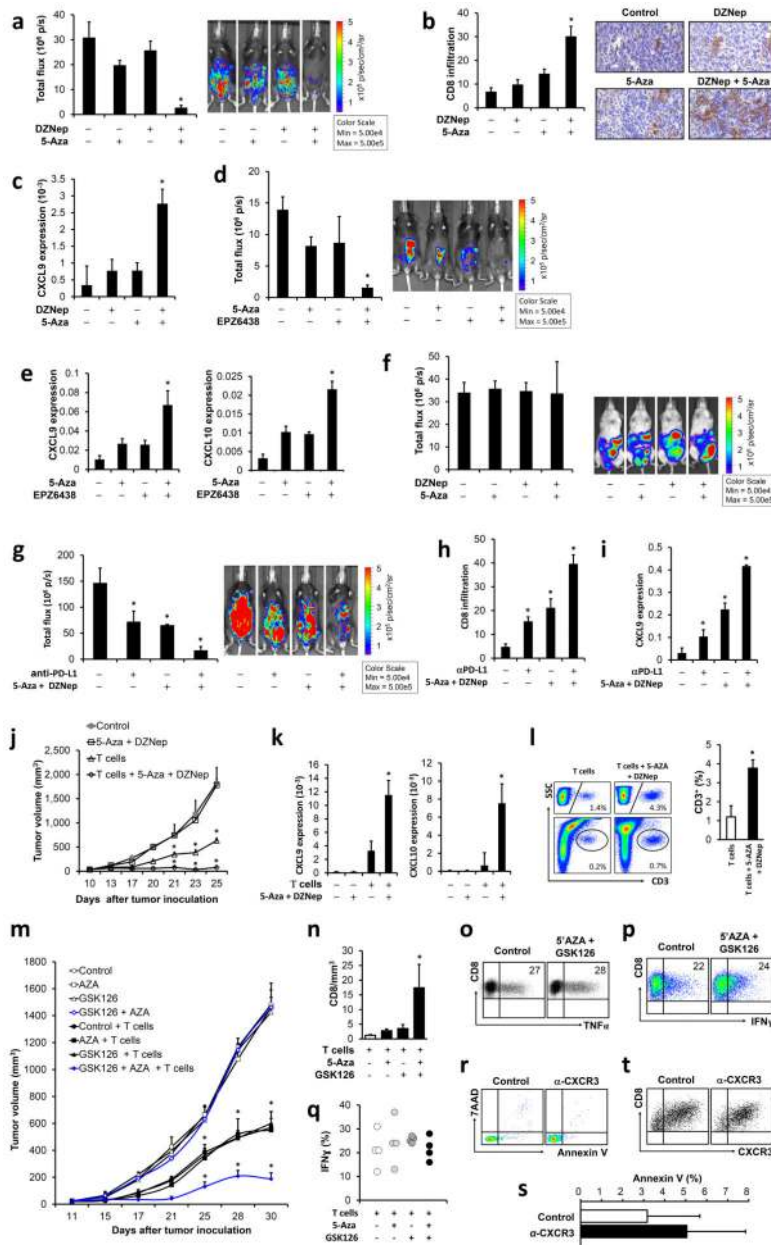
Extended Data Figure 1. Epigenetic reprogramming alters immunotherapy
a–c, Effects of DZNep and 5-AZA dC on ID8 mouse ovarian cancer progression. The ID8 tumor bearing mice (C57BL/6) were treated with DZNep and 5-AZA dC. (**a**) Tumor growth was recorded by Bioluminescence imaging and quantified by calculating the total flux (photons per second). The representative images and tumor volume at day 24 are shown. Day 0: tumor inoculation. (**b**) Tumor-infiltrating CD8^{+} T cells were quantified by immunohistochemistry staining (IHC) and expressed as the mean ± SEM per high-power field. (**c**) Tumor CXCL9 mRNA was quantified by real-time PCR. (mean/SEM, n = 5 per

group, * *P* < 0.05, Mann-Whitney Test as compared to the control group or the group treated with DZNep or 5-AZA dC).

d, e, Effects of EPZ6438 and 5-AZA dC on ID8 mouse ovarian cancer progression. The ID8 tumor bearing mice (C57BL/6) were treated with EPZ6438 and 5-AZA dC. (**d**) Tumor growth was recorded by Bioluminescence imaging and quantified by calculating the total flux (photons per second). The representative images and tumor volume at day 22 are shown. Day 0: tumor inoculation. (mean/SEM, * *P* < 0.05, One-way ANOVA). (**e**) Tumor CXCL9 mRNA was quantified by real-time PCR. (mean/SEM, * *P* < 0.05, One-way ANOVA).

f, Effects of DZNep and 5-AZA dC on ovarian tumor progression in NOD-scid/IL-2Rγnull (NSG) mouse. Mouse ID8-luc ovarian cancer cells were intraperitoneally inoculated into NSG mice. Tumor-bearing mice were treated with DZNep and 5-AZA dC. Tumor growth was recorded and quantified by Bioluminescence imaging. The representative bioluminescence images on day 15 (days after tumor inoculation) are shown. n = 4 per group. (mean/SEM).

g–i, Effects of DZNep and 5-AZA dC on anti-PD-L1 immunotherapy. Anti-PD-L1 (10mg/kg) was given to ID8 tumor bearing mice (C57BL/6) with or without DZNep and 5-AZA dC (5-Aza). (**g**) Tumor growth was recorded. The representative images and tumor volume at day 18 are shown. (**h**) Tumor-infiltrating CD8+ T cells were assessed and expressed as the mean ± SEM per high-power field. (**i**) Tumor CXCL9 gene expression was quantified and expressed as the mean values ± SEM. (n = 5 per group, **P* < 0.05, Mann-Whitney Test)

j–l, Effects of DZNep and 5-AZA dC on T cell immunotherapy. Autologous human tumor-specific human CD8+ T cells were transfused into ovarian cancer-bearing NOD-scid IL2Rγc null (NSG) mice with or without DZNep and 5-AZA dC treatment. The mice were treated with anti-CXCR3. Tumor volume was monitored (**j**). Th1-type chemokine expression was quantified by real-time PCR (**k**). Tumor-infiltrating T cells (**l**) were determined by FACS. (mean/SEM, n = 5 per group, * *P* < 0.05 Mann-Whitney Test).

m–q, Effects of GSK126 and 5-AZA dC on T cell immunotherapy. Ovarian cancer-bearing NSG mice were treated with or without GSK126 and 5-AZA dC, and received autologous human ovarian cancer-specific CD8+ T cell transfusion. Tumor volume (**m**), tumor-infiltrating T cells (**n**) and T cell cytokine profile (**o–q**) were shown (mean/SEM, n = 5 per group, * *P* < 0.05 Mann-Whitney Test). Total tumor-infiltrating CD8+ T cells were normalized to the tumor volume (absolute number of CD8+ T cells/mm^3 of the tumor). T cell cytokine profile was determined by FACS via gating on human CD45+CD8+ cells in tumor tissues. The percentages of TNFα+ and IFNγ+ cells are shown in CD8+ cells. Circle represents each mouse from the group. One of two experiments is shown.

r–t, Effects of anti-CXCR3 on T cell survival. Tumor-specific human CD8+ T cells were transfused into NSG mice. The mice were treated with anti-CXCR3. Peripheral blood Annexin V+CD8+ human T cells (mean/SEM, n = 5 per group) (**r, s**) and spleen CXCR3+CD8+ human T cells (**t**) were determined by FACS.
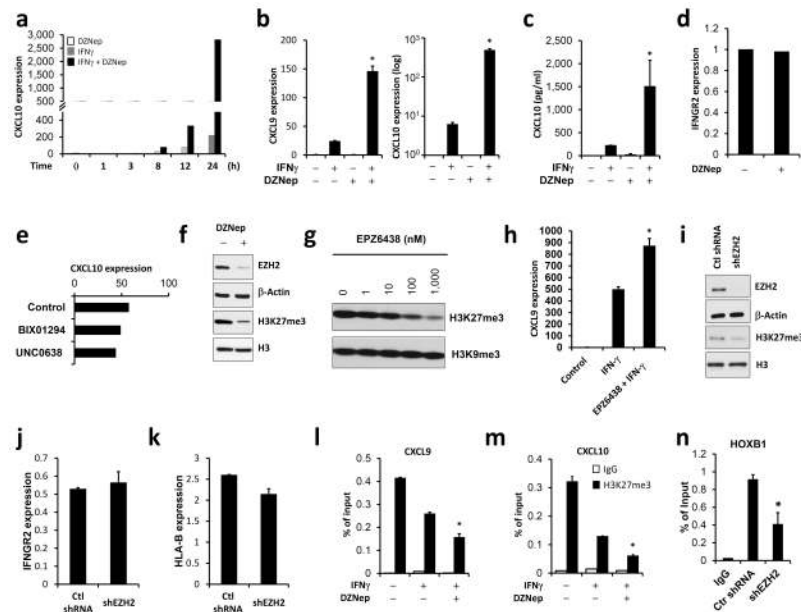
Extended Data Figure 2. EZH2 controls Th1-type chemokines

a, Effect of DZNep on CXCL10 transcript expression. Primary ovarian cancer cells were treated with DZNep in the presence of IFNγ for different time (hours). CXCL10 gene expression was quantified by real-time PCR. One of three experiments is shown.

b, c, Effects of DZNep on ovarian cancer Th1-type chemokine expression. Human primary ovarian cancer cells were treated for 24 (**b**) or 48 (**c**) hours with DZNep in the presence of IFNγ. CXCL9 and CXCL10 expression were quantified by real-time PCR (**b**) or detected by ELISA (**c**). (mean/SEM, n = 5, * *P* < 0.05, Wilcoxon test)

d, Effects of DZNep on IFNGR2 transcript expression. Primary ovarian cancer cells were treated with DZNep in the presence of IFNγ for 24 hours. IFNGR2 expression was quantified by real-time PCR. One of 3 experiments is shown.

e, Effects of histone methyltransferase G9a/GLP inhibitors on Th1-type chemokine expression. Primary ovarian cancer cells were treated with BIX01294 or UNC0638 in the presence of IFNγ for 24 hours. CXCL10 gene expression was quantified by real-time PCR. One of 3 experiments is shown.

f, Effects of DZNep on the expression of EZH2 and H3K27me3. Primary ovarian cancer cells were treated with or without DZNep for 24 hours. The levels of EZH2, H3K27me3 were detected by Western blotting. One of 3 experiments is shown.

g, h, Effects of EPZ6438 on histone marks (**g**) and CXCL9 mRNA expression (**h**). Mouse ID8 ovarian cancer cells were treated with EPZ6438 in the presence or absence of IFNg for 48 hours. H3K27me3 and H3K9me2 were detected by Western blotting. CXCL9 transcripts were quantified by real-time PCR. (Mean/SEM, 4 repeats, * *P* < 0.05, Wilcoxon test)

i, EZH2 knockdown in primary ovarian cancer cells mediated by EZH2 shRNA. Primary ovarian cancer cells were stably transduced with a lentiviral shRNA expressing vector (non-target shRNA (Ctl) or EZH2 shRNA, shEZH2). The levels of EZH2 and H3K27me3 were detected by Western Blotting.

j, k, Effects of EZH2 knockdown on IFNGR2 and HLA-B gene expression. Primary ovarian cancer cells were stably transduced with non-target shRNA (Ctl) or EZH2 shRNA

(shEZH2). IFNGR2 (**j**) and HLA-B (**k**) gene expression were quantified by real-time PCR. (mean/SEM, n = 4)

l, m, Effect of DZNep on H3K27me3 occupancy at Th1-type chemokine promoters. H3K27me3 ChIP assay was performed in primary ovarian cancer cells treated with DZNep with or without IFNγ. H3K27me3 levels at the gene promoter of CXCL9 and CXCL10 were normalized to the input. (mean/SEM, n = 5, * $P < 0.05$, Wilcoxon test)

n, Effects of EZH2 knockdown on H3K27me3 occupancy at the HOXB1 gene promoter. H3K27me3 ChIP assay was performed in shEZH2 or non-target shRNA expressing primary ovarian cancer cells. H3K27me3 levels at the gene promoter of HOXB1 were normalized to the input. (mean/SEM, n = 5, * $P < 0.05$, Wilcoxon test)
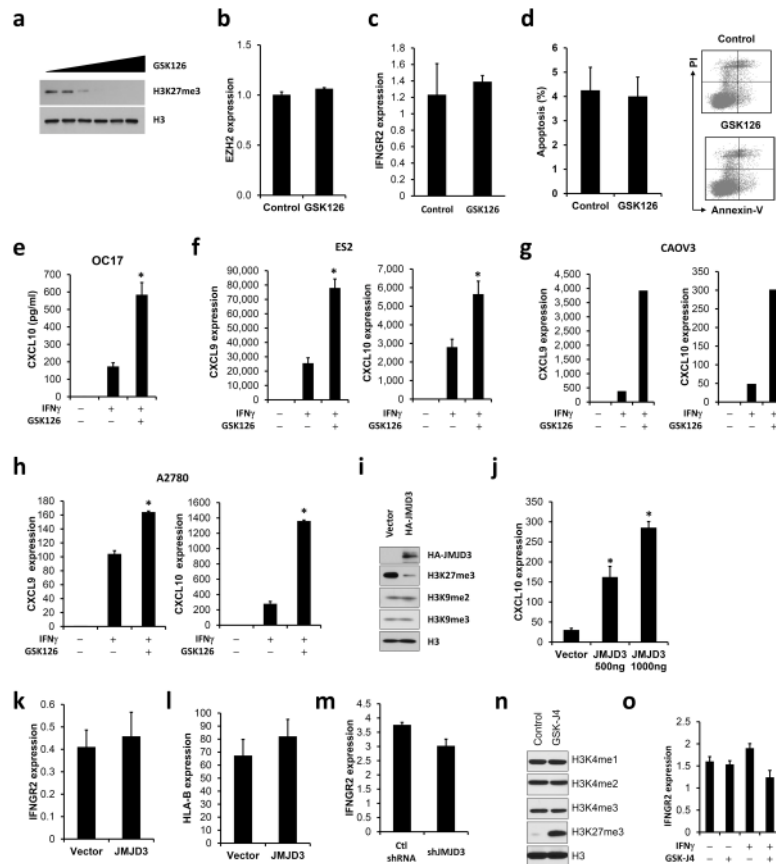
Extended Data Figure 3. H3K27-specific methyltransferase and demethylase regulates Th1-type chemokine expression

a, Effects of GSK126 treatment on H3K27me3. Primary ovarian cancer cells were treated with GSK126 (0, 0.05, 0.2, 0.5, 2 and 10 μM) for 48 hours. H3K27me3 was detected by Western Blotting. One of 3 experiments is shown.

b, c, Effects of GSK126 on EZH2 and IFNGR2 transcripts expression. Primary ovarian cancer cells were pretreated with GSK126 for 48 hours and stimulated with IFNγ for additional 24 hours. EZH2 (**b**) and IFNGR2 (**c**) transcripts were quantified by real-time PCR. Results are expressed as the mean ± SEM. 3 experiments with duplicates.

d, Effects of GSK126 on cell apoptosis. Primary ovarian cancer cells were treated with GSK126 and stained with PI and Annexin-V. The percentage of apoptotic cells (Annexin-V positive) was quantified. mean/SEM in 3 experiments with duplicates.

e–h, Effects of histone methyltransferase inhibitors on ovarian cancer Th1-type chemokine expression. Human primary ovarian cancer cells (OC17) (**e**), or ovarian cancer cell lines (ES-2, CAOV3 and A2780) (**f–h**) were treated with GSK126 with or without IFNγ. CXCL9 and CXCL10 expression was measured by ELISA (**e**) or real-time PCR (**f–h**). (mean/SEM, n = 5, * $P < 0.05$, Wilcoxon test)

i, Effects of ectopic JMJD3 on histone marks. Primary ovarian cancer cells were transiently transfected with plasmid encoding HA-JMJD3. Histone markers H3K9me2, H3K9me3 and H3K27me3 were detected by Western Blotting. One of 3 experiments is shown.

j, Effect of ectopic expression of JMJD3 on CXCL10 transcripts expression. Primary ovarian cancer cells were transiently transfected with vector or different amounts of HA-JMJD3 plasmids and stimulated with IFNγ. CXCL10 transcripts were quantified by real-time PCR. Results are expressed as the mean values ± SEM. Data represent 3 independent experiments. (n = 5, * $P < 0.05$, Wilcoxon test)

k, l, Effects of ectopic JMJD3 on IFNGR2 (**k**) and HLA-B (**l**) gene expression. Primary ovarian cancer cells were transiently transfected with plasmid encoding HA-JMJD3 and stimulated with IFNγ. IFNGR2 and HLA-B transcripts were quantified by real-time PCR. Results are expressed as the mean relative ± SEM. Data represent 3 independent experiments.

m, Effects of JMJD3 knockdown on IFNGR2 gene expression. Primary ovarian cancer cells were stably transduced with a lentiviral shRNA specific for JMJD3 (shJMJD3) or non-target shRNA (Ctl), and stimulated with IFNγ. IFNGR2 transcripts were quantified by real-time PCR. Results are expressed as the mean values ± SEM. Data represent 3 independent experiments.

n, Effects of GSK-J4 on histone marks. Primary ovarian cancer cells were treated with GSK-J4 (10 μM) for 48 hours. H3K27me3, H3K4me1, H3K4me2 and H3K4me3 were detected by Western Blotting. One of 3 experiments is shown.

o, Effects of GSK-J4 on IFNGR2 gene expression. Primary ovarian cancer cells were pretreated with GSK-J4 (10 μM) for 48 hours and stimulated with IFNγ for additional 24 hours. IFNGR2 transcripts were quantified by real-time PCR. Results are expressed as the mean values ± SEM. Data represent 3 independent experiments.
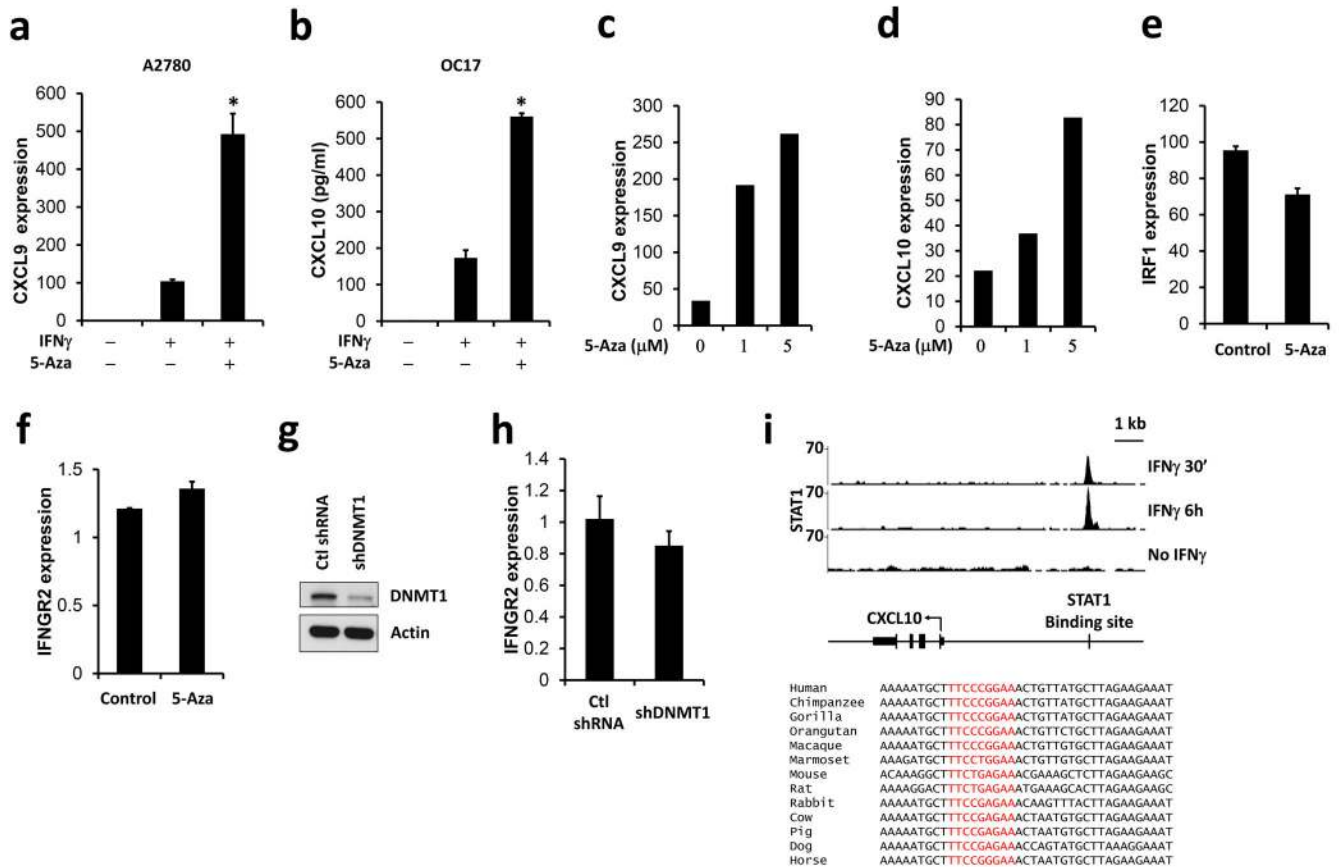
Extended Data Figure 4. DNA methylation controls Th1-type chemokine expression

a, b, Effects of 5-AZA dC on Th1-type chemokine expression. Human ovarian cancer cell line (A2780) or primary ovarian cancer cells (OC17) were treated with 5-AZA dC and IFNγ. CXCL9 and CXCL10 expression were quantified by real-time PCR (**a**) or ELISA (**b**). (mean/SEM, n = 6, * $P < 0.05$, Wilcoxon test)

c–f, Effects of 5-Aza dC on IFNγ associated gene expression. Primary ovarian cancer cells (OC8) were treated with 5-AZA dC and IFNγ for 24 hours. CXCL9 (**c**), CXCL10 (**d**), IRF1 (**e**) and IFNGR2 (**f**) transcripts were quantified by real-time PCR. Results are expressed as the mean values ± SEM. One of 3 independent experiments is shown.

g, DNMT1 knockdown via DNMT1 shRNA. Primary ovarian cancer cells (OC8) were transduced with a lentiviral shRNA specific for DNMT1 (shDNMT1) or non-target shRNA (Ctl). DNMT1 was detected by Western Blotting.

h, Effect of DNMT1 knockdown on IFNGR2 expression. Primary ovarian cancer cells (OC8) were transduced with a lentiviral shRNA specific for DNMT1 (shDNMT1) or non-target shRNA (Ctl) and stimulated with IFNγ for 24 hours. IFNGR2 transcripts were quantified by real-time PCR. Results are expressed as the mean values ± SEM. Data represent 3 independent experiments.

i, STAT1 binding site at CXC10 gene promoter. STAT1 ChIP-seq dataset from ENCODE/ SYDH (Top panel). K562 cells were treated with IFNγ for 30 minutes or 6 hours. Non-treated GM12878 cells were used as control (no IFNγ). GEO accession #: GSM935487, GSM935488 and GSM935612. STAT1 occupancy at CXCL10 promoter (−5143 to −4699) is

shown as the peaks. Middle panel, schematic diagram of CXCL10 gene locus. STAT1-binding site (TTCCCGGAA) were predicted by TFSEARCH, score = 100. STAT1 ChIP-seq peaks overlap with the predicted STAT1-binding site (indicated as vertical lines). Bottom, homologous STAT1 binding site at CXCL10 gene promoter (Ensemble Genomic alignment).
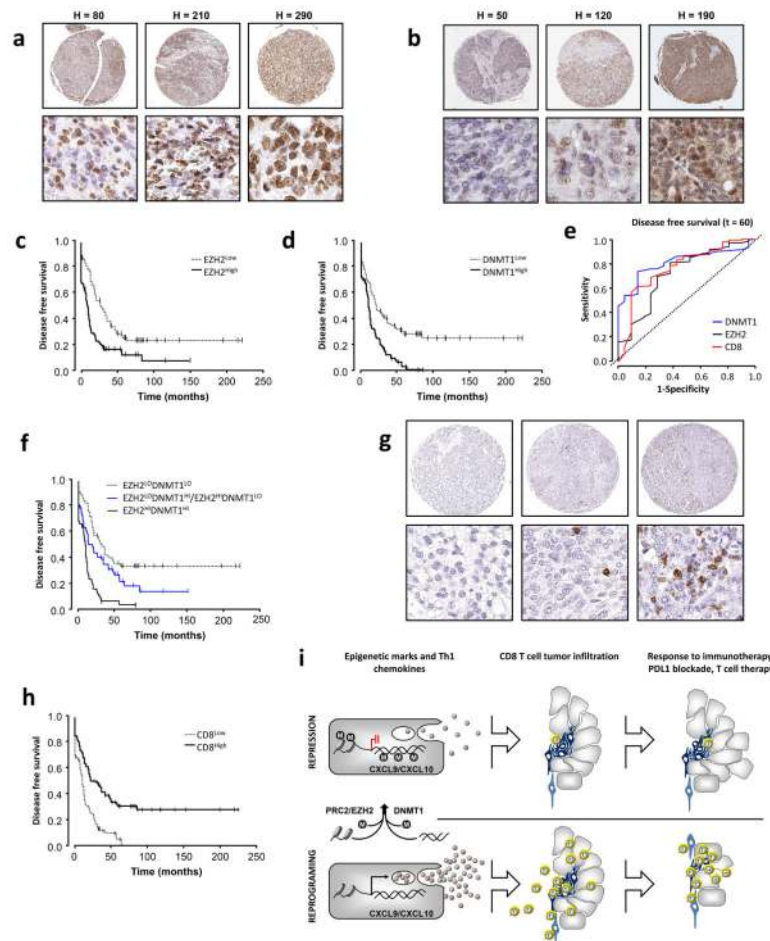
Extended Data Figure 5. EZH2/H3K27 and DNMT1 interaction affects clinical outcome

a–b, Representative images of immunohistochemistry staining of EZH2 (**a**) and DNMT1 (**b**) in human ovarian cancer tissues. The levels of DNMT1 and EZH2 expression in the tumor were assessed by H-score method.

c–d, The association between EZH2 (**c**), DNMT1 (**d**) and patient disease free survival in high-grade serous ovarian cancer. The high and low levels of EZH2 and DNMT1 were determined by the median values (see Extended Data Table 1).

e, Relative impact of EZH2, DNMT1 and CD8 on patient disease free survival in high-grade serous ovarian cancer. The time-dependent receiver operating characteristic (ROC) curve analysis was applied to evaluate the predictive accuracy of each marker for disease free survival. AUC, the area under the ROC curve. (T = 60).

f, Impact of the two parameters (EZH2 and DNMT1) on patient disease free survival. The analysis was performed on patients with high-grade serous ovarian cancer. Multiple

comparisons were performed in long-rank test. EZH2^{low}DNMT1^{low} group (n = 49) vs EZH2^{high}DNMT1^{high} (n = 55) P < 0.00001.

g, Representative images of immunohistochemistry staining of CD8 in human ovarian cancer specimen. Intratumoral CD8$^+$ T cells were shown with anti-CD8$^+$ staining. The numbers of intratumoral CD8$^+$ T cells were quantified in high power fields (40X). (See Methods and Extended Data Table 1).

h, The relationship between intratumoral CD8$^+$ T cells and patient disease free survival in high-grade serous ovarian cancer. (See Methods and Extended Data Table 1).

i, Schematic diagram depicting the relationship among epigenetic Th1-type chemokine silencing, effector T cell trafficking, and tumor immunity, immunotherapy and patient outcome.

Extended Data Table 1

Patient characteristics and risk factors for OS and DFS

		N	P	Hazard Ratio	95% Hazard Ratio Confidence Limits	
Overall survival						
Age: mean (min-max)	59 (19–87)	186	0.004	1.020	1.006	1.033
	I, II	30 (16%)				
Stage	III, IV	152 (82%)	0.0004	2.955	1.627	5.367
	ND	4 (2%)				
EZH2 *	High	103	< 0.0001	3.019	2.083	4.376
	Low	83				
DNMT1 *	High	90	< 0.0001	3.49	2.383	5.11
	Low	83				
CD8 *	High	97	< 0.0001	0.263	0.181	0.384
	Low	89				
Disease free survival						
Age: mean (min-max)	59 (19–87)	178	0.01	1.016	1.004	1.029
	I, II	28 (16%)				
Stage	III, IV	146 (82%)	0.0004	2.739	1.572	4.772
	ND	4 (2%)				
EZH2 *	High	99	< 0.0001	2.112	1.487	2.998
	Low	79				
DNMT1 *	High	86	< 0.0001	2.08	1.46	2.964
	Low	80				
CD8 *	High	90	< 0.0001	0.422	0.298	0.598
	Low	88				

Note: Univariate analysis.

*
Categorized values of EZH2, DNMT1 and CD8 are based on the median.

Extended Data Table 2

Risk factors for OS and DFS

Risk factors	P-value	Hazard ratio (HR)	95% HR Confidence Limits	
Overall survival				
EZH2*	**< 0.0001**	**2.657**	**1.817**	**3.884**
Age	0.0435	1.014	1	1.029
Stage	0.0236	2.038	1.1	3.776
DNMT1*	**< 0.0001**	**3.217**	**2.182**	**4.743**
Age	0.1096	1.011	0.998	1.025
Stage	0.0038	2.551	1.352	4.814
CD8*	**< 0.0001**	**0.31**	**0.211**	**0.455**
Age	0.117	1.011	0.997	1.024
Stage	0.0215	2.134	1.118	4.074
Disease free survival				
EZH2*	**0.0004**	**1.916**	**1.34**	**2.738**
Age	0.1321	1.01	0.997	1.024
Stage	0.0126	2.096	1.172	3.749
DNMT1*	**0.0004**	**1.929**	**1.344**	**2.77**
Age	0.0912	1.011	0.998	1.025
Stage	0.0116	2.104	1.181	3.748
CD8*	**<.0001**	**0.471**	**0.329**	**0.673**
Age	0.1653	1.009	0.996	1.022
Stage	0.0134	2.084	1.164	3.731

Note: Multivariate analysis

Extended Data Table 3

The nested multivariate models of OS and DFS

	DNMT1 AUC ± s.e.	EZH2 AUC ± s.e	CD8 AUC ± s.e
Overall survival	82.66 ± 3.34	83.63 ± 3.53	75.13±4.18
Disease free survival	81.06 ±3.91	71.98 ±6.28	76.53 ± 5.86

Extended Data Table 4

The AUC values of ROCs (t=60) for DNMT1, EZH2 and CD8

Gene	Sequence (5′-3′)	Sequence (5′-3′)
Primers for quantitative Real-Time PCR		
Human CXCL10	CTCCAGTCTCAGCACCATGA	GCTCCCCTCTGGTTTTAAGG
Human CXCL9	GTGGTGTTCTTTTCCTCTTGGG	ACAGCGACCCTTTCTCACTAC
Human IFNGR2	TTCACTGCCGCCAGTCCCTCA	GGGAGCCTTCTCCTGGGGTCA
Human HLA-B	TCCTAGCAGTTGTGGTCATG	TCAAGCTGTGAGAGACACAT

Primers for quantitative Real-Time PCR		
Gene	**Sequence (5′-3′)**	**Sequence (5′-3′)**
Human EZH2	TTCATGCAACACCCAACACTT	GGTGGGGTCTTTATCCGCTC
Human IRF1	GAGACCCTGGCTAGAGATGC	CATGGCACAGCGAAAGTTGG
Mouse CXCL10	AATGAGGGGCCATAGGGAAGC	AGCCATCCACTGGGTAAAGG
Mouse CXCL9	GAGCAGTGTGGAGTTCGAGG	TCCGGATCTAGGCAGGTTTG

Primers for ChIP assay		
Gene	**Sequence (5′-3′)**	**Sequence (5′-3′)**
CXCL10	GGAATGTCTCAGAAAACGTGGGGC	ACCTTCGAGTCTGCAACATGGGA
CXCL9	AGGGTTTCCCCCAGCACAATCA	ACCAGCAAGATGATGCCCAAGAGG
HOXB1	GGGTTGGGAGGGAAGGAAAG	CCCATCCATCTGAGAGCGAC

Lentiviral shRNA		
shRNA	**Vector**	**Source**
shEZH2	pGreen-shEZH2-1	Kindly provided by Dr. Arul Chinnaiyan
	pGreen-shEZH2-2	Kindly Provided by Dr. Arul Chinnaiyan
shJMJD3	pGIPz-shJMJD3 (V3LHS_301324)	Vector Core (University of Michigan)
	pGIPz-shJMJD3 (V3LHS_310328)	Vector Core (University of Michigan)
shDNMT1	pGIPZ-DNMT1_V2LHS_113503	Vector Core (University of Michigan)
	pGIPZ-DNMT1_V2LHS_113505	Vector Core (University of Michigan)

Extended Data Table 5

Sequences for ChIP, PCR primers and lentiviral shRNAs

Overall survival models	P value	likelihood rate statistics
DNMT1 and EZH2 vs. DNMT1 alone*	< 0.0001	35.5
DNMT1 and EZH2 vs. EZH2 alone*	< 0.0001	47.2

Disease free survival	P value	likelihood rate statistics
DNMT1 and EZH2 vs. DNMT1 alone*	< 0.0001	16.6
DNMT1 and EZH2 vs. EZH2 alone*	< 0.0001	17

Acknowledgments

References

1. Timp W, Feinberg AP. Cancer as a dysregulated epigenome allowing cellular growth advantage at the expense of the host. Nature reviews. Cancer. 2013; 13:497–510. [pii]. DOI: 10.1038/nrc3486nrc3486

2. Curiel TJ, et al. Blockade of B7-H1 improves myeloid dendritic cell-mediated antitumor immunity. Nat Med. 2003; 9:562–567. [PubMed: 12704383]

3. Zou W, Chen L. Inhibitory B7-family molecules in the tumour microenvironment. Nat Rev Immunol. 2008; 8:467–477. [PubMed: 18500231]

4. Pardoll DM. The blockade of immune checkpoints in cancer immunotherapy. Nature reviews. Cancer. 2012; 12:252–264. [pii]. DOI: 10.1038/nrc3239nrc3239 [PubMed: 22437870]

5. Rosenberg SA, Restifo NP, Yang JC, Morgan RA, Dudley ME. Adoptive cell transfer: a clinical path to effective cancer immunotherapy. Nature reviews Cancer. 2008; 8:299–308. [PubMed: 18354418]

6. Spranger S, Bao R, Gajewski TF. Melanoma-intrinsic beta-catenin signalling prevents anti-tumour immunity. Nature. 2015; 523:231–235. [PubMed: 25970248]

7. Scholler J, et al. Decade-long safety and function of retroviral-modified chimeric antigen receptor T cells. Sci Transl Med. 2012; 4:132ra153. [pii].

8. Brentjens RJ, et al. CD19-targeted T cells rapidly induce molecular remissions in adults with chemotherapy-refractory acute lymphoblastic leukemia. Sci Transl Med. 2013; 5:177ra138. [pii].

9. Tan J, et al. Pharmacologic disruption of Polycomb-repressive complex 2-mediated gene repression selectively induces apoptosis in cancer cells. Genes Dev. 2007; 21:1050–1063. [PubMed: 17437993]

10. Knutson SK, et al. Selective inhibition of EZH2 by EPZ-6438 leads to potent antitumor activity in EZH2-mutant non-Hodgkin lymphoma. Molecular cancer therapeutics. 2014; 13:842–854. [PubMed: 24563539]

11. Cui TX, et al. Myeloid-derived suppressor cells enhance stemness of cancer cells by inducing microRNA101 and suppressing the corepressor CtBP2. Immunity. 2013; 39:611–621. [pii]. DOI: 10.1016/j.immuni.2013.08.025S1074-7613(13)00377-4 [PubMed: 24012420]

12. Curiel TJ, et al. Specific recruitment of regulatory T cells in ovarian carcinoma fosters immune privilege and predicts reduced survival. Nat Med. 2004; 10:942–949. [pii]. DOI: 10.1038/nm1093nm1093 [PubMed: 15322536]

13. Kryczek I, et al. B7-H4 expression identifies a novel suppressive macrophage population in human ovarian carcinoma. The Journal of experimental medicine. 2006; 203:871–881. [PubMed: 16606666]

14. Kryczek I, et al. Human TH17 Cells Are Long-Lived Effector Memory Cells. Sci Transl Med. 2011; 3:104ra100. 3/104/104ra100 [pii].

15. McCabe MT, et al. EZH2 inhibition as a therapeutic strategy for lymphoma with EZH2-activating mutations. Nature. 2012; 492:108–112. [pii]. DOI: 10.1038/nature11606nature11606 [PubMed: 23051747]

16. Zhang Y, et al. The polycomb repressive complex 2 governs life and death of peripheral T cells. Blood. 2014; 124:737–749. [PubMed: 24951427]

17. Cao R, Zhang Y. The functions of E(Z)/EZH2-mediated methylation of lysine 27 in histone H3. Curr Opin Genet Dev. 2004; 14:155–164. [PubMed: 15196462]

18. Agger K, et al. UTX and JMJD3 are histone H3K27 demethylases involved in HOX gene regulation and development. Nature. 2007; 449:731–734. DOI: 10.1038/nature06145 [PubMed: 17713478]

19. Kruidenier L, et al. A selective jumonji H3K27 demethylase inhibitor modulates the proinflammatory macrophage response. Nature. 2012; 488:404–408. [pii]. DOI: 10.1038/nature11262nature11262 [PubMed: 22842901]

20. Heagerty PJ, Lumley T, Pepe MS. Time-dependent ROC curves for censored survival data and a diagnostic marker. Biometrics. 2000; 56:337–344. [PubMed: 10877287]

21. Zhang L, et al. Intratumoral T cells, recurrence, and survival in epithelial ovarian cancer. The New England journal of medicine. 2003; 348:203–213. [PubMed: 12529460]

22. Galon J, et al. Type, density, and location of immune cells within human colorectal tumors predict clinical outcome. Science. 2006; 313:1960–1964. [PubMed: 17008531]

23. Doege CA, et al. Early-stage epigenetic modification during somatic cell reprogramming by Parp1 and Tet2. Nature. 2012; 488:652–655. nature11333 [pii]. DOI: 10.1038/nature11333 [PubMed: 22902501]

24. Mansour AA, et al. The H3K27 demethylase Utx regulates somatic and germ cell epigenetic reprogramming. Nature. 2012; 488:409–413. nature11272 [pii]. DOI: 10.1038/nature11272 [PubMed: 22801502]

25. Tumeh PC, et al. PD-1 blockade induces responses by inhibiting adaptive immune resistance. Nature. 2014; 515:568–571. [PubMed: 25428505]

26. Zitvogel L, Kepp O, Kroemer G. Decoding cell death signals in inflammation and immunity. Cell. 2010; 140:798–804. [PubMed: 20303871]

27. Park S, et al. The therapeutic effect of anti-HER2/neu antibody depends on both innate and adaptive immunity. Cancer Cell. 2010; 18:160–170. S1535-6108(10)00248-5 [pii]. DOI: 10.1016/j.ccr.2010.06.014 [PubMed: 20708157]

28. Twyman-Saint Victor C, et al. Radiation and dual checkpoint blockade activate non-redundant immune mechanisms in cancer. Nature. 2015; 520:373–377. [PubMed: 25754329]

29. Tran E, et al. Cancer immunotherapy based on mutation-specific CD4+ T cells in a patient with epithelial cancer. Science (New York, N Y). 2014; 344:641–645.

30. Gubin MM, et al. Checkpoint blockade cancer immunotherapy targets tumour-specific mutant antigens. Nature. 2014; 515:577–581. [PubMed: 25428507]

31. Zou W, et al. Stromal-derived factor-1 in human tumors recruits and alters the function of plasmacytoid precursor dendritic cells. Nat Med. 2001; 7:1339–1346. [PubMed: 11726975]

32. Kryczek I, et al. IL-22CD4 T Cells Promote Colorectal Cancer Stemness via STAT3 Transcription Factor Activation and Induction of the Methyltransferase DOT1L. Immunity. 2014

33. Kryczek I, et al. Expression of aldehyde dehydrogenase and CD133 defines ovarian cancer stem cells. Int J Cancer. 2012; 130:29–39. DOI: 10.1002/ijc.25967 [PubMed: 21480217]

34. Roby KF, et al. Development of a syngeneic mouse model for events related to ovarian cancer. Carcinogenesis. 2000; 21:585–591. [PubMed: 10753190]

35. LIN DY, WEI LJ, YING Z. Checking the Cox model with cumulative sums of martingale-based residuals. Biometrika. 1993; 80:557–572. DOI: 10.1093/biomet/80.3.557
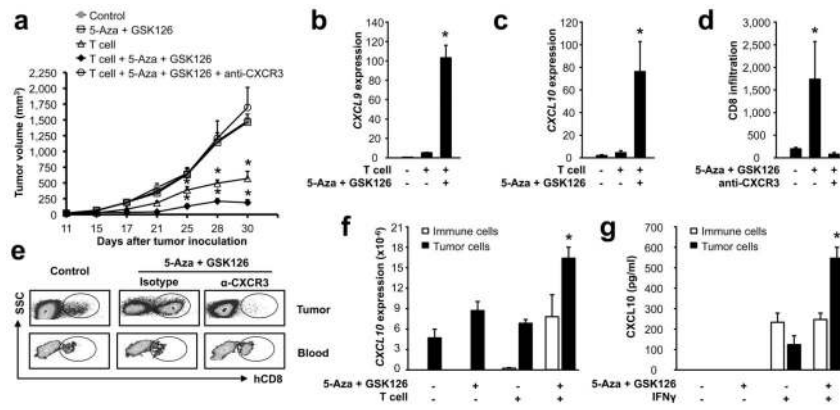
Figure 1. Epigenetic reprogramming alters cancer T cell immunotherapy
Effects of GSK126 and 5-AZA dC on T cell immunotherapy. Ovarian cancer-bearing NSG mice were treated with GSK126, 5-AZA dC and/or anti-CXCR3, and received TAA-specific CD8^{+} T cell transfusion. Tumor volume (**a**), tumor chemokine expression (**b, c**), tumor-infiltrating T cells and blood T cells (**d, e**) were shown. CXCL10 transcript was quantified in tumor and immune cells from tumor tissues in NSG model (**f**). Tumor and immune cells (10^6/ml) were isolated from ovarian cancer from patients, and were treated for 48 hours in the indicated conditions. CXCL10 protein was measured by ELISA (**g**) (mean/SD, n = 5, * P < 0.05, Mann-Whitney Test).
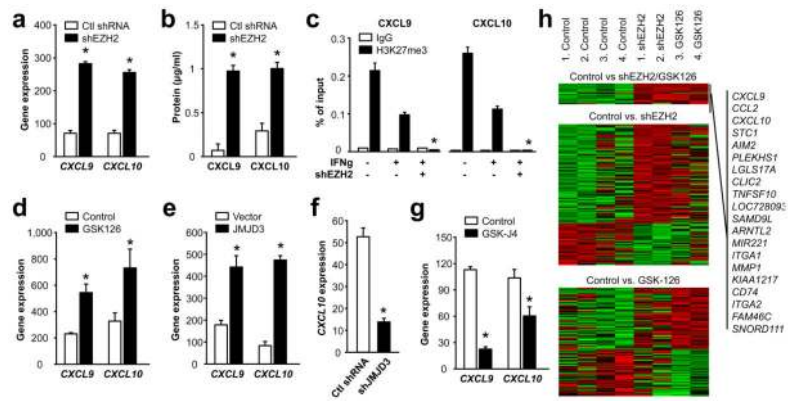
Figure 2. Histone methyltransferase represses Th1-type chemokines

a, b, Effects of EZH2 knockdown on cancer Th1-type chemokine expression. shEZH2 and control vector expressing primary ovarian cancer cells were stimulated with IFNγ, and chemokines were quantified by real-time PCR (**a**) or ELISA (**b**). (mean/SD, n = 6, * $P <$ 0.05, Wilcoxon test)

c, Effect of shEZH2 on H3K27me3 occupancy at Th1-type chemokine promoters. H3K27me3 ChIP was performed in shEZH2 expressing primary ovarian cancer cells. H3K27me3 levels at the gene promoter of CXCL9 and CXCL10 were normalized to the input. (mean/SD, n = 5, * $P <$ 0.05, Wilcoxon test)

d, Effects of GSK126 on cancer Th1-type chemokine expression. Primary ovarian cancer cells were pretreated with GSK126 and stimulated with IFNγ for 24 hours. Chemokine transcripts were quantified by real-time PCR. (mean/SEM, n = 6, * $P <$ 0.05, Wilcoxon test)

e–g, Effects of JMJD3 on cancer Th1-type chemokine expression. Primary ovarian cancer cells were transfected with plasmids encoding HA-JMJD3 (**e**), or with a lentiviral shJMJD expressing vector (**f**) or pretreated with GSK-J4 (**g**), and stimulated with IFNγ for 24 hours. Chemokine transcripts were quantified by real-time PCR. (mean/SD, n = 5, *$P <$ 0.05, Wilcoxon test)

h, Effects of EZH2 and H3K27me3 manipulation on global changes of gene expression. Primary ovarian cancer cells were treated with GSK126, or transduced with a shEZH2 lentivirus, and stimulated with IFNγ. Heat map shows differential up-regulation and down-regulation of genes in GSK126 treated cells and in shEZH2 cells compared to the controls. The 20 overlapped differentially expressed genes in both shEZH2 and GSK126 treated cells were shown on the top. Two repeats/condition.
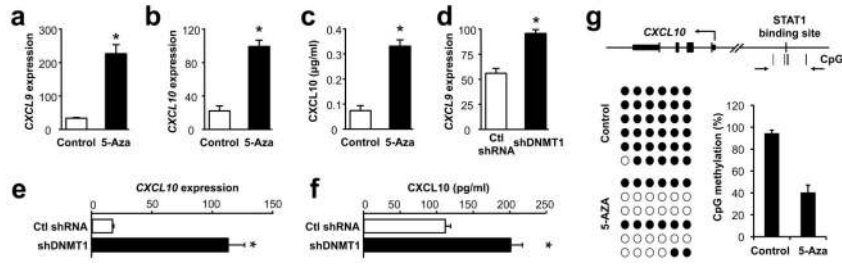
Figure 3. DNA methylation regulates Th1-type chemokine expression

a–c, Effects of 5-AZA dC on Th1-type chemokine expression. Primary ovarian cancer cells were treated with 5-AZA dC and IFNγ for 24 (**a, b**) or 48 hours (**c**). CXCL9 and CXCL10 transcripts (**a, b**) and protein (**c**) were quantified by real-time PCR or ELISA. (mean/SD, n = 7, * P < 0.05, Wilcoxon test)

d–f, Effects of shDNMT1 on Th1-type chemokine expression. Primary ovarian cancer cells were transduced with shDNMT1 or non-target shRNA and stimulated with IFNγ. Chemokine transcript (**d, e**) and protein (**f**) were quantified by real-time PCR and ELISA. (mean/SEM, n = 5, * P < 0.05, Wilcoxon test)

g, Effects of 5-AZA dC on DNA methylation on the promoter of CXCL10 gene. Schematic diagram of *CXCL10* gene locus is shown (Top). Primary ovarian cancer cells were treated with 5-AZA dC. DNA methylation at CpG sites was quantified by bisulfite sequencing. Results are shown as the percentage of methylation. Filled circle, methylated; open circle, unmethylated. The arrows indicate the locations of primers.
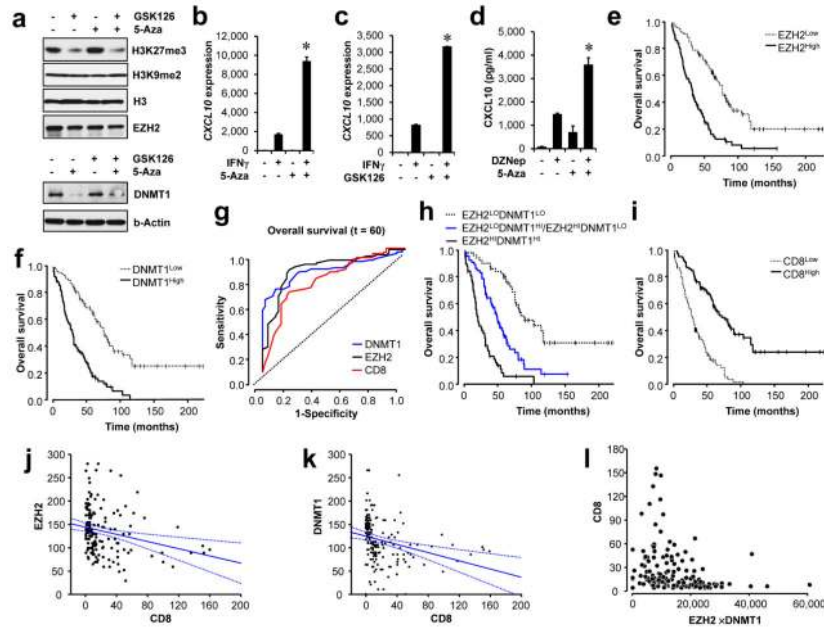
Figure 4. EZH2/H3K27 and DNMT1 interaction and its impact on clinical outcome

a, Effects of GSK126 and 5-AZA dC on H3K27me3 and DNMT1. Primary ovarian cancer cells were treated with GSK126 or/and 5-AZA dC for 48 hours. Histone marks and DNMT1 were detected by Western Blotting.

b, c, d Effects of 5-AZA dC and GSK126 on tumor CXCL10. shEZH2 (**b**), shDNMT1 (**c**) and primary (**d**) ovarian cancer cells were treated with 5-AZA dC for 2 days (**b, c**) or with DZNep and/or 5-AZA dC for 3 days (**d**), followed by IFNγ stimulation. CXCL10 was quantified by real-time PCR (**b, c**) and ELISA (**d**). (mean/SEM, n = 5–6, * $P < 0.05$, Wilcoxon test)

e, f, The association between EZH2 (**e**), DNMT1 (**f**) and OS. $P < 0.0001$.

g, Impact of EZH2, DNMT1 and $CD8^+$ T cells on OS. The ROC curve analysis was applied to evaluate the predictive accuracy of each marker for OS. (T = 60)

h, Impact of EZH2 and DNMT1 on OS. EZH2^{low}DNMT1^{low} (**n = 50**), EZH2^{high}DNMT1^{high} (**n = 57**), EZH2^{low}DNMT1^{high}, and EZH2^{high}DNMT1^{low} (**n = 66**) were compared. Long-rank test, $P < 0.0001$, EZH2^{low}DNMT1^{low} vs EZH2^{high}DNMT1^{high}.

i, The relationship between intratumoral $CD8^+$ T cells and OS. $P < 0.0001$.

j, k, l, The Pearson correlation between intratumoral $CD8^+$ T cells and EZH2 (n = 169, r = −0.24, $P = 0.002$) (**j**) and DNMT1 (n = 170, r = −0.28, $P = 0.0003$) (**k**) and the accumulating levels of EZH2 and DNMT1 (n = 168, r = −0.32, $P < 0.0001$) (**l**).